

Temporal label recovery from noisy dynamical data

Yuehaw Khoo, Xin T. Tong, Wanjie Wang, and Yuguan Wang

June 21, 2024

Abstract

Analyzing dynamical data often requires information of the temporal labels, but such information is unavailable in many applications. Recovery of these temporal labels, closely related to the seriation or sequencing problem, becomes crucial in the study. However, challenges arise due to the nonlinear nature of the data and the complexity of the underlying dynamical system, which may be periodic or non-periodic. Additionally, noise within the feature space complicates the theoretical analysis. Our work develops spectral algorithms that leverage manifold learning concepts to recover temporal labels from noisy data. We first construct the graph Laplacian of the data, and then employ the second (and the third) Fiedler vectors to recover temporal labels. This method can be applied to both periodic and aperiodic cases. It also does not require monotone properties on the similarity matrix, which are commonly assumed in existing spectral seriation algorithms. We develop the ℓ_∞ error of our estimators for the temporal labels and ranking, without assumptions on the eigen-gap. In numerical analysis, our method outperforms spectral seriation algorithms based on a similarity matrix. The performance of our algorithms is further demonstrated on a synthetic biomolecule data example.

1 Introduction

The dynamical data, where the objects evolve, is observed in many scientific fields. Examples include the evolution data of fossils, movement data of robots, and protein folding data at varying time points. The statistical interest is to recover the evolving pattern from the dynamic data. Depending on specific fields, plenty of models and algorithms have been developed, examples including the time series models (Tsay, 2005; Wang et al., 2015; Hamilton, 2020), data assimilation (Law et al., 2015; Asch et al., 2016), and neural networks (Bailer-Jones et al., 1998; Selvin et al., 2017).

Let $X(t) \in \mathbb{R}^d$ denote the underlying dynamic system at time t , where $t \in [0, 2\pi]$. While we call t as “time”, it may denote time, angle, or other factors that vary upon the system (Singer & Shkolnisky, 2011; Moscovich et al., 2020). In practice, we make observations on N discrete time points t_i , $i \in [N]$. Let $e_i \in \mathbb{R}^p$ denote the observational noise at each time point t_i . The observed data points are $Z_i = X(t_i) + e_i$, $i \in [N]$.

In most existing algorithms, knowing the temporal labels $t_{[N]}$ is crucial for analyzing dynamic data $Z_{[N]}$. However, $t_{[N]}$ is often missing in practice, making it vital

to recover $t_{[N]}$. In cryo-electron microscopy (cryo-EM), one hopes to reconstruct a 3D molecular structure from many 2D images of a molecule in various directions. However, if the molecule undergoes molecular dynamics, even when the view directions of the images are known, one still needs to identify each image with a different molecular conformation (i.e., temporal label t_i) to prevent blurring in the reconstruction (Moscovich et al., 2020; Lederman et al., 2020; Seitz et al., 2022). This gives rise to a time-labeling problem. Moreover, recovering temporal labels of the images allows reconstruction of the conformation trajectory, which could be pivotal in advancing cryo-EM as a tool to study molecular dynamics and molecular energy landscape (Cossio et al., 2022; Vant et al., 2022). Similarly, in embryo development research, samples are collected at different growth stages, but these stages t_i are not explicitly identified. Determining t_i is critical for understanding and modeling embryo development (Jaeger et al., 2004; Dsilva et al., 2015). In metagenomics and bioinformatics, the well-known genome assembly problem requires an ordering of short DNA samples to reconstruct the original DNA sequences, analogous to recovering t_i (Brown et al., 2016; Ma et al., 2021a,b). These challenges are also present in other fields such as paleontology and archeology (Shennan, 1997; O’Brien & Lyman, 1999).

Recovery of the temporal label is closely related to the seriation/sequencing problem. The latter concerns how to order all data points $Z_{[N]}$ in a linear order. If we can obtain the temporal label $t_{[N]}$, the ordering of $Z_{[N]}$ can be determined by the ordering of $t_{[N]}$. In Arabie et al. (1996), the seriation problem is solved by minimizing a loss function over all possible permutations of $[N]$. Exact optimization has a huge time cost at $O(N!)$. The time cost is reduced by follow-up works, such as the dynamical programming approach in Hubert et al. (2001), the branch-and-bound approach in Brusco et al. (2005), and more simplifications in Hahsler et al. (2008). Nevertheless, at the beginning of Hahsler et al. (2008), the authors indicate their seriation algorithm is meant for a sample size of around 40. This is insufficient in the age of big data.

Efficient algorithms have been introduced in recent years. One direction is to use spectral methods. In detail, the pairwise similarity matrix is constructed based on $Z_{[N]}$. The graph Laplacian matrix is then calculated and its Fiedler vector (the eigenvector with the second smallest eigenvalue) is used for seriation. Assuming the similarity matrix has a monotone structure, Atkins et al. (1998) shows that the entries of the Fiedler vector increase/decrease monotonically in the noiseless case. Therefore, sorting the Fiedler vector gives the correct ordering of data. Fogel et al. (2014) extends this algorithm to the noisy data. Ma et al. (2021a) considers a special case where the underlying noiseless matrix has monotone rows on the order of interest. With this property, Ma et al. (2021a) proposes a more efficient estimation scheme, with further extensions in Ma et al. (2021b) and Cai & Ma (2023) to handle extreme values and double-sided ordered data. The most complicated case is in Rigollet & Weed (2019), where the data has nonlinear monotone dependence on the order. All these methods require the data or matrix entries to have a monotone or even linear dependence on the underlying ordering. However, this assumption may not hold in practice for complex nonlinear data.

The temporal label recovery problem faces a complex data structure. As t increases, $X(t)$ may be non-periodic or periodic. If $\{X(t)\}_{t \in [0, 2\pi]}$ has two disjoint endpoints with no self-loops, then we call it an *open curve*. Such a pattern can be found in the seriation settings and the evolution example. For biomolecule structures, their possible

conformations may form a periodic dynamical system suggesting a *closed loop*, where $X(0) = X(2\pi)$; see Yoshida et al. (2001) and Zelesko et al. (2019). Methods and derivations differ in these two cases. Second, in the era of big data, we have a large sample size N and a large dimension d of the feature space. The algorithm efficiency is important, as well as the statistical convergence under the noise.

To solve the time-label recovery problem, we borrow ideas from manifold learning and spectral seriation algorithms. Despite the high-dimensional feature space, the intrinsic dimension of $\{X(t)\}_{t \in [0, 2\pi]}$, viewed as a manifold, is one. For one-dimensional manifolds, the eigenfunctions of manifold Laplacian are simple trigonometric functions of t ; see (Rosenberg, 1997). The inverse of these eigenfunctions maps certain values to t . The problem is to figure out these certain values for each data point. From the pairwise similarity matrix of $Z_{[N]}$ based on the Gaussian kernel, the graph Laplacian is constructed and its Fiedler eigenvectors can be used to obtain a low-dimensional representation of the data. The Fiedler eigenvectors converge to the eigenfunctions of the manifold Laplacian when the Gaussian kernel bandwidth $\sigma \rightarrow 0$ and sample size $N \rightarrow \infty$; see Coifman & Lafon (2006) and Singer (2006). We leverage these insights to derive a new spectral algorithm to recover the temporal labels t_i by the Laplacian's Fiedler eigenvectors.

To establish the theoretical guarantee of the algorithm, the convergence of Laplacian Fiedler eigenvectors to the eigenfunctions is required. Singer (2006) establishes the asymptotic convergence of graph Laplacian towards manifold Laplacian. García Trillos et al. (2020) discusses the spectral convergence for a compact manifold (closed loop) case with no noise. Cheng & Wu (2022) extends the study to the noisy case and allows the appearance of eigenvalue multiplicity. Peoples & Harlim (2021) discusses the open curve case, with noiseless assumption. The convergence in all these works is in the context of ℓ_2 norm, and Dunson et al. (2021) gives the convergence in ℓ_∞ for the closed loop case without noise. Unfortunately, these settings are too simple for the time-label recovery problem.

We provide the spectral convergence in ℓ_∞ norm, which works for both the open curve and closed loop cases, in the presence of high-dimensional noise e_i and eigenvalue multiplicity. Our study suggests that

- for the closed loop case, the ℓ_∞ error has the same order as the ℓ_2 error;
- for the open curve case, the ℓ_∞ error is significantly smaller than the ℓ_2 error in Peoples & Harlim (2021), if both endpoints are excluded.

The result in the open curve case may seem counter-intuitive since ℓ_∞ error is a stronger bound. It holds because large errors in the eigenvector estimation occur near the boundary, and our analysis can capture this delicate fact. Meanwhile, we would like to point out that our analysis is based on a very different framework. In particular, the matrix we analyze does not have a low-rank part with a nondegenerate eigenvalue gap, which is commonly assumed in other papers, such as Abbe & Sandon (2015); Cai & Zhang (2018); Chen et al. (2021).

2 Methods: Laplacian ordering

2.1 Data and notations

The collected data points are $Z_i \in \mathbb{R}^d$, $i \in [N]$. Denote $Z = (Z_1, \dots, Z_N) \in \mathbb{R}^{d \times N}$ as the matrix form. For each data point Z_i , there is an underlying temporal label t_i to recover. Our goal is to recover $t_{[N]}$ and an ordering π of Z_i , so that $\pi(i) < \pi(j)$ if and only if $t_i < t_j$. The latter is known as the seriation problem.

The relationship between Z_i and t_i is captured by a dynamical system $\{X(t)\}_{t \in \mathbb{R}}$, where $X(t) \in \mathbb{R}^d$. Without loss of generality, we assume $t \in [0, 2\pi]$. Z_i is comprised by $X(t_i)$ and the observation error $e_i \in \mathbb{R}^d$, i.e. $Z_i = X(t_i) + e_i$. For notation simplicity, we let $X_i = X(t_i)$ and $X = (X_1, \dots, X_N) \in \mathbb{R}^{d \times N}$ be the matrix form. Let \mathcal{M} denote the manifold that the curve $X(t)$ lies in. The dimension of \mathcal{M} is 1. It motivates us to use manifold learning to recover $t_{[N]}$.

Throughout the paper, for a vector a , we use $\|a\|$ and $\|a\|_\infty$ to denote the ℓ_2 norm and ℓ_∞ norm of a . For a matrix A , $\|A\|$ and $\|A\|_F$ refer to its spectral norm and Frobenius norm, respectively. For an integer N , write $[N] = \{1, 2, \dots, N\}$. Let $1_{i=j}$ to be the indicator function.

2.2 Spectral seriation in the noiseless case

We begin with the ideal case where the clean data X is known, without concerns about the noise vector e_i . In this noiseless case, recovering t_i remains challenging due to the nonlinear relationship between $X(t)$ and t . We borrow the ideas in manifold learning to overcome this challenge. Since \mathcal{M} has a dimension of 1, eigenfunctions of the manifold Laplacian of \mathcal{M} are simple trigonometric functions of t . These eigenfunctions can be used to recover t_i .

The manifold \mathcal{M} is parameterized as $\{X(t)\}_{t \in [0, 2\pi]}$. Depending on $X(0) = X(2\pi)$ or not, \mathcal{M} can be either a closed loop or an open curve in \mathbb{R}^d . We discuss the two cases separately. For the open curve case $X(0) \neq X(2\pi)$, \mathcal{M} is not periodic. The eigenfunction of the Laplacian on \mathcal{M} is $\cos(t/2)$, which is monotone for $t \in [0, 2\pi]$. Estimating $\hat{v}_i = \cos(t_i/2)$ directs to an estimate $\hat{t}_i = \arccos(\hat{v}_i)$. For the closed loop case that $X(0) = X(2\pi)$, $X(t)$ is periodic. Two eigenfunctions of the Laplacian on \mathcal{M} , $\cos(t)$ and $\sin(t)$, are used to identify a specific $t_i \in [0, 2\pi]$. Therefore, to recover the temporal label t_i , we only need to recover the eigenfunction values corresponding to each data point X_i .

To recover the eigenfunctions, we investigate the eigenvectors of graph Laplacian of X . Define the Gaussian kernel with bandwidth $\sigma > 0$ as

$$k(x, y; \sigma) = (\sqrt{2\pi}\sigma)^{-1} \exp(-(2\sigma^2)^{-1}\|x - y\|^2). \quad (1)$$

Using this kernel, we set up the similarity between each two data points, i.e. $k(X_i, X_j; \sigma)$. We build two variants of the graph Laplacian and use different recovery functions under the open curve case and the closed loop case.

Consider the open curve case first. Define the normalized Laplacian $L^X \in \mathbb{R}^{N \times N}$

as follows,

$$L^X(i, j; \sigma) = 1_{i=j} - k(X_i, X_j; \sigma) \left(\frac{1}{2d^X(i)} + \frac{1}{2d^X(j)} \right), \quad d^X(i) = \sum_{j \in [N]} k(X_i, X_j; \sigma). \quad (2)$$

Denote λ_k^X as the k -th smallest eigenvalue of L^X , where $\lambda_1^X = 0$. Denote $F^X \in \mathbb{R}^N$ to be the Fiedler eigenvector, i.e., the eigenvector associated to λ_2^X .

When the bandwidth $\sigma \rightarrow 0$ and $N \rightarrow \infty$, it is known that the Fiedler vector F^X converges to the discretized eigenfunction $\cos(t/2)$ up to a sign shift. In other words, with high probability, $F^X(i) \approx N^{-1/2} \cos(t_i/2)$, $i \in [N]$. A natural estimation follows, that

$$\hat{t}_i(X) = \arccos(\sqrt{N} F^X(i)). \quad (3)$$

Further, ranking $\hat{t}_i(X)$ in ascending/descending order yields an ordering of the data points, which is the estimation of ranking $\hat{\pi}(X)$. The theoretical guarantee can be found in Peoples & Harlim (2021), which gives the convergence rate between F^X and the discretized eigenfunction in ℓ_2 norm, as a function of σ and N .

Now consider the closed loop case, where \mathcal{M} is a compact manifold. For this case, the normalized Laplacian is defined as

$$L^X(i, j; \sigma) = 1_{i=j} - k(X_i, X_j; \sigma) / \sqrt{d^X(i)d^X(j)}, \quad d^X(i) = \sum_{j \in [N]} k(X_i, X_j; \sigma). \quad (4)$$

Denote λ_k^X as the k -th smallest eigenvalue of L^X , where $\lambda_1^X = 0$. Denote F_+^X and $F_-^X \in \mathbb{R}^N$ to be the Fiedler eigenvectors, i.e., the eigenvectors associated with λ_2^X and λ_3^X . The discretized eigenfunctions are that $\cos(t_i)$ and $\sin(t_i)$. However, since \mathcal{M} is a closed loop, the starting point $X(0)$ can be any point on this curve. For example, the new parameterization starts at $\tilde{X}(0) = X(t_0)$, then the corresponding discretized eigenfunctions are $\cos(t_i - t_0)$ and $\sin(t_i - t_0)$. Similarly, a reflection will cause the same problem. Therefore, the convergence and recovery of t_i are discussed up to a rotation or a rotation-reflection.

Up to rotation or rotation-reflection, $F_+^X(i)$ and $F_-^X(i)$ converge to $c \cos(t_i)$ and $c \sin(t_i)$ respectively, where c is a constant. To get rid of c , we normalize F_+^X and F_-^X to recover $\cos(t_i)$ and $\sin(t_i)$, that

$$\cos(\hat{t}_i^X) = F_+^X(i) / \sqrt{\{F_+^X(i)\}^2 + \{F_-^X(i)\}^2}, \quad \sin(\hat{t}_i^X) = F_-^X(i) / \sqrt{\{F_+^X(i)\}^2 + \{F_-^X(i)\}^2}.$$

By $\cos(\hat{t}_i^X)$ and $\sin(\hat{t}_i^X)$, $\hat{t}_i^X \in [0, 2\pi]$ can be uniquely recovered. Ordering it in an ascending/descending order gives the ranking of data points $\hat{\pi}$. The convergence rate has been discussed in García Trillos et al. (2020) on the ℓ_2 norm and Dunson et al. (2021) in the ℓ_∞ norm.

2.3 Algorithm: spectral seriation on noisy dynamical data

The analysis in the noiseless case sheds light on the temporal label recovery of noisy data. We first construct the normalized Laplacian matrix L^Z , by replacing X_i to be

Z_i in Equations (2) and (4). The second (and third) Fiedler vectors are then used to recover the temporal labels. In detail, we first find out the similarity $k(Z_i, Z_j; \sigma)$ by the Gaussian kernel with bandwidth σ , and then calculate the degree $d^Z(i) = \sum_{j \in [N]} k(Z_i, Z_j; \sigma)$. The Laplacian matrix L^Z and Fiedler vectors F^Z naturally follow. The detailed algorithms are presented as Algorithm 1 for the open curve case and Algorithm 2 for the closed loop case.

Algorithm 1 *Temporal label recovery and ordering for non-periodic data.*

Input: Data Z ; Gaussian kernel bandwidth σ .

1. Compute the graph Laplacian L^Z , where $L^Z(i, j) = 1_{i=j} - k(Z_i, Z_j; \sigma) \left(\frac{1}{2d^Z(i)} + \frac{1}{2d^Z(j)} \right)$.
2. Let F^Z be the eigenvector of L^Z that corresponding to the second smallest eigenvalue.
3. Estimate $\hat{t}_i = 2 \arccos(\sqrt{N} F^Z(i))$.
4. Find a sorting $\hat{\pi}$ of $\hat{t}_{[N]}$ so that $\hat{t}_{\hat{\pi}(i)}$ is increasing in i .

Output: estimated time stamp $\hat{t}_{[N]} \in [0, 2\pi]$ and the ranking $\hat{\pi}$.

Algorithm 2 *Temporal label recovery and ordering for periodic data.*

Input: Data Z ; Gaussian kernel bandwidth σ .

1. Compute the graph Laplacian L^Z , where $L^Z(i, j) = 1_{i=j} - k(Z_i, Z_j; \sigma) / \sqrt{d^Z(i)d^Z(j)}$.
2. Find the second and third smallest eigenvalue, and its eigenvectors F_+^Z and F_-^Z of L^Z .
3. Find $\hat{t}_i \in [0, 2\pi]$ so that $\cos(\hat{t}_i) = \frac{F_+^Z(i)}{\sqrt{(F_+^Z(i))^2 + (F_-^Z(i))^2}}$, $\sin(\hat{t}_i) = \frac{F_-^Z(i)}{\sqrt{(F_+^Z(i))^2 + (F_-^Z(i))^2}}$.
4. Find a sorting $\hat{\pi}$ of $\hat{t}_{[N]}$ so that $\hat{t}_{\hat{\pi}(i)}$ is increasing in i .

Output: estimated time stamp $\hat{t}_{[N]} \in [0, 2\pi]$ and the ranking $\hat{\pi}$.

Remark 1 Say that ϵ is approximately the magnitude of error between Z_i and $X(t_i)$. For the periodic data, a suggested choice of the bandwidth is $\sigma = \max\{N^{-1/7}, \epsilon^{1/4}\}$, which is suggested in Theorem 2. For the non-periodic data, the suggested bandwidth is $\sigma = \max\{N^{-1/14}, \epsilon^{2/7}\}$; see Theorem 4.

Remark 2 For the open curve case, t_i 's are identifiable up to a reflection, i.e. the direction of the curve. For the closed loop case, t_i 's are identifiable up to a rotation and a rotation-reflection, i.e. the direction of the loop and the starting point of the loop. We want to point out that since $\{X(t)\}_{t \in \mathbb{R}}$ is periodic for the closed loop case, there are no natural starting or ending points. Identifying \hat{t}_i up to a rotation is sufficient to recover the dynamical system.

3 Theoretical Guarantee

3.1 Dynamical model with unknown timelabels

To introduce the theoretical results of spectral seriation algorithms, we first set up the assumptions on the dynamical system $\{X(t)\}_{t \in [0, 2\pi]}$ and noise. Recall that \mathcal{M} is the manifold formed by $\{X(t)\}_{t \in [0, 2\pi]}$ and the observed data points are $Z_i = X(t_i) + e_i$, $i \in [N]$. Assumptions are posed on the manifold \mathcal{M} , the noise $e_{[N]}$, and the temporal labels $t_{[N]}$.

Assumption 1 \mathcal{M} is a 1D manifold isometrically embedded in \mathbb{R}^d . In particular, there is a constant $L_{\mathcal{M}} > 0$, so that for any two points $x, y \in \mathcal{M}$ and $d_{\mathcal{M}}(x, y)$ denoting the distance between x and y on \mathcal{M} , there is $\|x - y\| \leq d_{\mathcal{M}}(x, y) \leq \|x - y\|(1 + L_{\mathcal{M}}\|x - y\|^2)$.

Assumption 2 The time points t_i 's follow the uniform distribution on $[0, 2\pi]$ for $i \in [N]$.

Assumption 3 There is a constant $\epsilon > 0$, so that $\sup_{i \in [N]} \|Z_i - X(t_i)\| \leq \epsilon$.

Assumption 1 requires the system $X(t)$ to be a regular isometric embedding to estimate. Here $L_{\mathcal{M}}$ measures (upper bounds) the curvature of the embedding. Assumption 2 assumes a uniform distribution of the time points for simplicity. It guarantees the whole curve to be covered. Assumption 3 assumes a uniform bound on the magnitude of noise. In more challenging settings, say a diverging d , one may need to denoise the data so that Assumption 3 holds. A brief discussion on data denoising algorithm and theoretical results can be found in Appendix A.

In the following context, L^Z denotes the graph Laplacian constructed on the data Z by Algorithms 1 and 2, varying on the scenarios. $F_j^Z \in \mathbb{R}^N$ denotes the eigenvector of L^Z corresponding to the j -th smallest eigenvalue. We say $a_N = \tilde{O}(b_N)$ or $a_N \lesssim b_N$, if there are universal constants C and m so that $a_N \leq C(\log N)^m b_N$ for $N \rightarrow \infty$.

3.2 Statistical error: closed loop

When \mathcal{M} is a closed loop, there are no natural starting or ending points. In other words, $t_{[N]}$ is identifiable up to a rotation and a rotation-reflection. To measure the errors, we define $[a]_{2\pi}$ to be the representative of a within the interval $[-\pi, \pi)$ under modulo 2π , for any constant a . For two time sequences $t_{[N]}$ and $t'_{[N]}$, we define the distance between them by minimizing all possible rotational matching or reflexive rotational matching, i.e.

$$Err(t_{[N]}, t'_{[N]}) = \min_{r=\pm 1, \theta \in [0, 2\pi]} \max_{i \in [N]} |[rt_i + \theta - t'_i]_{2\pi}|. \quad (5)$$

Here θ denotes the additional rotational angle, $r = 1$ leads to a matching without reflection, and $r = -1$ leads to a matching with an additional reflection.

In the evaluation of ranking $\pi'_{[N]}$, the rotation effect is captured by a shift n . The reflection effect in ranking is denoted as π_r where $\pi_r(i) = N - \pi(i)$. Let j represent the modular effect.

$$Err(\pi_{[N]}, \pi'_{[N]}) = \min_{\tilde{\pi} \in \{\pi, \pi_r\}, n \in [N]} \max_{i \in [N]} \min_{j \in \{0, \pm 1\}} \{|\tilde{\pi}(i) + n + jN - \pi'(i)|\}/N. \quad (6)$$

Both definitions concern the maximum error in the time sequence or the ranking, i.e. ℓ_∞ error. Bounding this error is both challenging and crucial, as it implies a consistent limit on estimation accuracy. Substituting the maximum with a summation in (5) yields the ℓ_2 error bound, which is discussed in Cheng & Wu (2022).

To prove the effectiveness of Algorithm 2, we first show the convergence of the Fiedler eigenvectors to the manifold eigenfunctions.

Theorem 1 [Convergence of Fiedler eigenvectors] *Suppose \mathcal{M} is a closed loop and Assumptions 1 – 3 are satisfied with a constant $\epsilon > 0$. Consider Algorithm 2 with a Gaussian bandwidth of $\sigma > 0$. Let F_j^Z be the j -th smallest eigenvector of L^Z , $j = 2, 3$, then with a high probability $1 - O(N^{-1})$, there is a constant $c > 0$, so that*

$$\min_{r=\pm 1, \theta \in [0, 2\pi]} \max_{i \in [N]} |\sqrt{N} F_j^Z(i) - c \cos((j-1)(rt_i + \theta))| = \tilde{O}(\sigma^{-2}\epsilon + \sigma^{-3/2}N^{-1/2} + \sigma^2),$$

where r and θ are the rotational and reflective parameters.

Theorem 2 *Under the same assumptions with Theorem 1, further suppose that the sample size N and the Gaussian kernel bandwidth σ satisfy that $N\sigma > 1$ and $\sigma < 1/L_{\mathcal{M}}$, then with a high probability $1 - O(N^{-1})$, the estimates $\hat{t}(Z)$ and $\hat{\pi}(Z)$ by Algorithm 2 satisfy that*

$$\begin{aligned} Err(\hat{t}_{[N]}, t_{[N]}) &\leq \tilde{O}(\sigma^{-2}\epsilon + \sigma^{-3/2}N^{-1/2} + \sigma^2), \\ Err(\hat{\pi}_{[N]}, \pi_{[N]}) &\leq \tilde{O}(\sigma^{-2}\epsilon + \sigma^{-3/2}N^{-1/2} + \sigma^2). \end{aligned}$$

These results establish the error bound of Algorithm 2 even when confronted with high-dimensional noise that $|Z_i - X(t_i)| \leq \epsilon d^{-1/2}$. The error bound depends on the noise level ϵ , sample size N , and the Gaussian kernel bandwidth σ employed in creating L^Z . The effects of dimensionality d have been removed by the denoising step, which results in an interesting phenomenon that the error bound does not depend on d .

Remark 3 *By Theorems 1 and 2, it is essential for the bandwidth σ to meet the conditions $\sigma > \epsilon^{1/2}$ and $\sigma > N^{-1/3}$ to effectively counter data noise. When N and ϵ are fixed, we would choose $\sigma = \max\{N^{-1/7}, \epsilon^{1/4}\}$ and reaches an error of order $\max\{N^{-2/7}, \epsilon^{1/2}\}$.*

Remark 4 *Consider two special cases. When there is no noise, i.e., $\epsilon = 0$, the ideal bandwidth is $\sigma = N^{-1/7}$, resulting in an accuracy of $\tilde{O}(N^{-2/7})$. This error rate mirrors that of García Trillos et al. (2020) in the noiseless scenario but considers the ℓ_2 error instead. Our approach achieves a uniform error bound that achieves the same error rate with the ℓ_2 error, which is remarkable. When the noise ϵ is fixed and the sample size $N \rightarrow \infty$, the optimal bandwidth $\sigma = \epsilon^{1/4}$ leads to accuracy of $\epsilon^{1/2}$. It can be seen as the “essential error” caused by noises.*

3.3 Statistical error: open curve

For an open curve \mathcal{M} with two separate endpoints, rotation is no longer a concern. Consequently, the time sequence $t_{[N]}$ can be identified up to a reflection. On the other hand, due to the limited number of samples near the endpoints, estimation on these temporal labels always has a large error. Hence, we evaluate the maximum error in time sequence estimation on the interior of the interval defined by a parameter δ , i.e. $int_\delta = [\delta, 2\pi - \delta]$. The definition is as follows.

$$E_{int_\delta}(t_{[N]}, t'_{[N]}) = \min \left\{ \max_{i:\delta < t_i < 2\pi - \delta} |t_i - t'_i|, \max_{i:\delta < t_i < 2\pi - \delta} |2\pi - t_i - t'_i| \right\}. \quad (7)$$

The maximum is over the temporal labels excluding the small regions around two endpoints, and the minimum considers the effects of a possible reflection.

When it comes to the ranking π , the ranks in consideration are $S_\delta(\pi) = \{i : N\delta \leq \pi(i) \leq N(1 - \delta)\}$. The distance between two rankings $\pi_{[N]}$ and $\pi'_{[N]}$ is defined as follows.

$$E_{int_\delta}(\pi_{[N]}, \pi'_{[N]}) = \min \left\{ \max_{i \in S_\delta(\pi)} |\pi(i) - \pi'(i)|, \max_{i \in S_\delta(\pi)} |N - \pi(i) - \pi'(i)| \right\}. \quad (8)$$

Theorem 3 *Suppose \mathcal{M} is an open curve and Assumptions 1–3 hold. Let F_j^Z be the j -th smallest eigenvector of L^Z for a fixed integer $j \in [N]$ by Algorithm 1, then with a high probability at least $1 - O(N^{-2})$,*

$$\min_{r \in \pm 1} \max_{\delta \leq t_i \leq 2\pi - \delta} |\sqrt{N}F_{j+1}^Z(i) - r \cos(jt_i/2)| = \tilde{O}(\sigma + \sigma^{-5/2}N^{-1/4} + \sigma^{-5/2}\epsilon),$$

where $\cos(jt_i/2)$ is an eigen-function of the manifold Laplacian.

Theorem 4 *Under the same assumptions with Theorem 3, further suppose that the sample size N and the Gaussian kernel bandwidth σ satisfy that $N\sigma > 1$ and $\sigma < 1/L_{\mathcal{M}}$, then with a high probability $1 - O(N^{-2})$, the estimates $\hat{t}(Z)$ and $\hat{\pi}(Z)$ by Algorithm 1 satisfy that*

$$\begin{aligned} E_{int_\delta}(t_{[N]}^Z, t_{[N]}) &\leq \tilde{O}(\sigma + \sigma^{-5/2}N^{-1/4} + \sigma^{-5/2}\epsilon), \\ E_{int_\delta}(\pi_{[N]}^Z, \pi_{[N]}) &\leq \tilde{O}(\sigma + \sigma^{-5/2}N^{-1/4} + \sigma^{-5/2}\epsilon). \end{aligned}$$

When the sample size N and the noise level ϵ are fixed, the optimal Gaussian kernel bandwidth is $\sigma = \max\{N^{-1/14}, \epsilon^{2/7}\}$, which yields an error of order $\max\{N^{-1/14}, \epsilon^{2/7}\}$. In the noiseless case that $\epsilon = 0$, the optimal bandwidth $\sigma = N^{-1/14}$ leads to an error at $\tilde{O}(N^{-1/14})$. When $N \rightarrow \infty$, then $\sigma = \epsilon^{2/7}$ yields an error at $\tilde{O}(\epsilon^{2/7})$. For the open curve case, more neighbors are required in the construction of L^Z and the convergence is slower than the closed loop case.

In Peoples & Harlim (2021), the ℓ_2 error is studied in the noiseless setting, where the rate is of $\tilde{O}(N^{-1/28})$. Surprisingly, our method yields an error rate of approximately $\tilde{O}(N^{-1/14})$, which is faster than the error in Peoples & Harlim (2021). This counterintuitive outcome stems from our error measurement (7), which excludes the endpoints. Notably, errors around the endpoints are substantial, contributing to a large overall error.

3.4 Getting the ℓ_∞ bound: a quick guide

Sections 3.2 and 3.3 provide insights into the ℓ_∞ perturbation bounds concerning the eigenvectors of L^Z . Such analysis on ℓ_∞ spectral perturbation bounds is gaining interest within the statistics community. Studies leverage leave-one-out analysis (Abbe et al., 2020) to transform the ℓ_2 eigenvector perturbation bound based on the Davis-Kahan theorem (Davis & Kahan, 1970), into an ℓ_∞ bound. This transformation guarantees robust strong consistency, a departure from classical consistency results that solely ensure average accuracy. In particular, one can obtain uniform error controls which is essential for certain statistical procedures. More details can be found in Tong et al. (2023) and Hu & Wang (2024).

In this section, we explain how to obtain an ℓ_∞ bound from an ℓ_2 error bound, which starts from the following simple reformulation.

Lemma 5 *Suppose F^Z is an eigenvector of L^Z with eigenvalue λ^Z . Let $Q^Z = I - L^Z$. Let Q_i^Z and L_i^Z denote the i -th row of Q^Z and L^Z , respectively. Consider a fixed index i . Suppose for a vector $v \in \mathbb{R}^N$ and some constants λ and $\delta_1, \delta_2, \delta_3 > 0$, the followings hold*

$$|(Q_i^Z)'(F^Z - v)| \leq N^{-1/2}\delta_1, |(L_i^Z)'v - \lambda v(i)| \leq N^{-1/2}\delta_2, |\lambda - \lambda^Z| |v(i)| \leq N^{-1/2}\delta_3.$$

Then there is

$$|F^Z(i) - v(i)| \leq (\delta_1 + \delta_2 + \delta_3) / \{\sqrt{N}(1 - \lambda^Z)\}.$$

Proof 1 F^Z is the eigenvector of L^Z with eigenvalue λ^Z , so $\lambda^Z F^Z = L^Z F^Z$, which leads to

$$\lambda^Z(F^Z - v) = \lambda^Z F^Z - \lambda^Z v = L^Z(F^Z - v) + L^Z v - \lambda^Z v \quad (9)$$

Take the i -th row of (9) and rearrange it,

$$(1 - \lambda^Z)\{v(i) - F^Z(i)\} = (Q_i^Z)'(v - F^Z) + \{(L_i^Z)'v - \lambda v(i)\} + (\lambda - \lambda^Z)v(i).$$

Dividing both sides by $1 - \lambda^Z$ and plugging in bounds from the conditions, the result is proved.

Apply Lemma 5 to the graph Laplacian L^Z defined in the algorithms, where the prescribed eigenvector v is taken as the discretized eigenfunctions of the manifold Laplacian, i.e. $v(i) \propto \cos(t_i/2)$ for the open curve case or $v(i) \propto \cos(t_i)$ for the closed loop case, and the constant λ is the eigenvalue corresponding to v . Our goal is to bound $\|F^Z - v\|_\infty$. By Lemma 5, the bound is based on $\|Q^Z(F^Z - v)\|_\infty$, $\|L^Z v - \lambda v\|_\infty$, and $|\lambda - \lambda^Z| \|v\|_\infty$.

Bounding the last two terms is not complicated, by existing results and the random matrix theory. For $|\lambda - \lambda^Z|$, Peoples & Harlim (2021) and Cheng & Wu (2022) have set the upper bound for $|\lambda - \lambda^X|$ and $|\lambda^X - \lambda^Z|$ is bounded by random matrix theory. The term $\|L^Z v - \lambda v\|_\infty$ evaluates the ‘‘error’’ when fitting λ and v in the eigenvector equation respective to L^Z , $L^Z v = \lambda v$. Since L^Z is a noisy and discretized version

of the manifold Laplacian, of which v is the true eigenvector, such an error can be well-bounded.

The challenging part is to bound the projection $\|Q^Z(F^Z - v)\|_\infty$. We first show that the naive Cauchy-Schwarz inequality does not work. For an index i , the Cauchy-Schwarz inequality gives $|(Q_i^Z)'(F^Z - v)| \leq \|Q_i^Z\| \|F^Z - v\|$, which means the product of $\max_i \|Q_i^Z\|$ and the ℓ_2 error bound of $F^Z - v$ will induce an upper bound on the ℓ_∞ error. In detail, we show that $\|Q_i^Z\| = \tilde{O}((N\sigma)^{-1/2})$ in the supplementary materials. $\|F^Z - v\| \leq \|F^Z - F^X\| + \|F^X - v\|$, where the effects of noise $\|F^Z - F^X\| = \tilde{O}(\epsilon/\sigma^2)$ by the Davis-Kahan Theorem. The effects of discretization $\|F^X - v\| = \tilde{O}(\sqrt{\sigma})$ for the open curve case, by Peoples & Harlim (2021). Introduce these terms into the Cauchy-Schwarz estimate gives $\|F^Z - v\|_\infty = \tilde{O}(N^{-1/2})$; this bound is at the same order with $\|v\|_\infty$ and cannot be used for study accuracy of $t_{[N]}^Z$. For the closed loop case, this naive Cauchy-Schwarz estimate gives a usable but weaker estimate than what we offer in theorems.

Our tight bound exploits the fact that F^Z is an eigenvector of L^Z and v is an approximate eigenvector of L^Z , corresponding to a small eigenvalue $\lambda^Z = O(\sigma^2)$. We relate the inner product $\langle Q_i^Z, F^Z - v \rangle$ to L^Z by a discretized Poisson's equation. Starting from a fixed index i , suppose there is a vector $U_i \in \mathbb{R}^N$ such that $L^Z U_i = Q_i^Z$, then the inner product

$$\langle Q_i^Z, F^Z - v \rangle = \langle L^Z U_i, F^Z - v \rangle = \langle U_i, L^Z(F^Z - v) \rangle \approx \lambda^Z \langle U_i, F^Z - v \rangle. \quad (10)$$

Since $\lambda^Z = O(\sigma^2)$ and $\|F^Z - v\|$ is bounded, a sharp uniform bound can be found if the $\|U_i\|$ is well-bounded for all $i \in [N]$.

Now the problem is to bound U_i where $L^Z U_i = Q_i^Z$ for $i \in [N]$. Suppose there exists a function ψ_i , so that $\psi_i(t_j) = U_i(j)$. Q_i^Z is close to the kernel matrix of Z up to a constant factor. It gives that $Q_i^Z(j) \approx \phi_i(t_j)$, where $\phi_i(t) = \sqrt{2\pi} \exp(-\sigma^{-2}\|t_i - t\|^2/2)$. Introduce these terms into the equation about U_i , then the goal is to find $\psi_i(t)$ so that

$$L^Z U_i \approx L^Z \psi_i(t_{[N]}) \approx \psi_i(t) - \mathbb{E}_{\xi \sim \mathcal{N}(0,1)}[\psi_i(t + \sigma\xi)] = \phi_i(t). \quad (11)$$

It is the Poisson equation about $\psi_i(t)$ and $\phi_i(t)$. The solution $\psi_i(t)$ can be explicitly written down as an infinite summation. By bounding the explicit terms in the summation, we can bound the vector $\psi_i(t)$ and then $\|U_i\|$. The rigorous analysis can be found in the supplementary materials.

4 Numerical experiments

4.1 Comparison with seriation methods

We compare our spectral seriation approach with traditional seriation methods using pairwise comparison data under a simplified setting that $d = 2$. We conduct two simulation studies when the underlying dynamic system $\{X(t)\}$ is: a) a half-circle $X(t) = (\cos(t), \sin(t))$ for $t \in [0, \pi]$; and b) $X(t) = (2 \cos(t) - 1 - \cos(2t), 2 \sin(t) -$

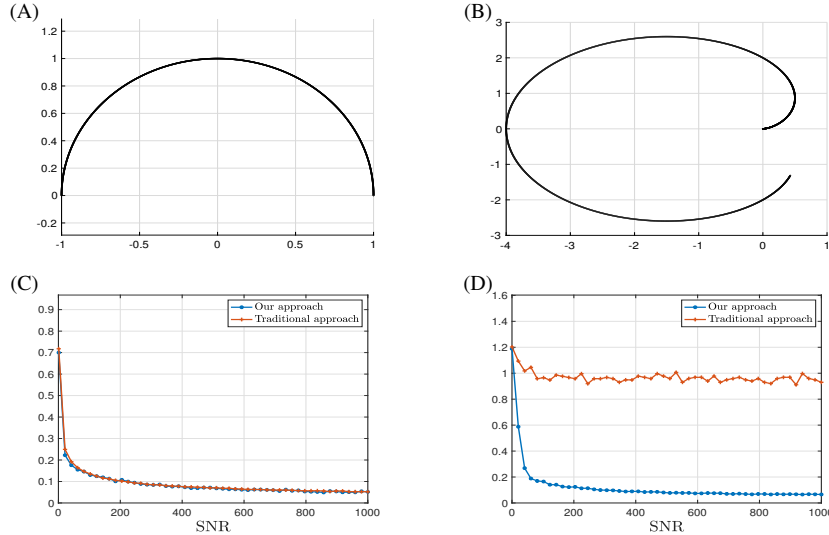


Figure 1: Dynamical systems \mathcal{M}_1 and \mathcal{M}_2 are shown in (A) and (B) respectively. Comparison of the relative errors of our approach (line with circles) and the approach in Fogel et al. (2014) (line with crosses) are shown in (C) (for \mathcal{M}_1) and (D) (for \mathcal{M}_2).

$\sin(2t)$ for $t \in [0, 8\pi/5]$. Both are open curves to facilitate the comparison of ranking. The manifolds are shown in Figure 1.

We start by randomly drawing $N = 2000$ temporal labels, t_i , from $(0, \pi)$ for 1) or $(0, 8\pi/5)$ for 2). The clean data matrix X have rows $X_i = X(t_i)$, $i \in [N]$. We then introduce noise to X and form the data $Z = X + \mathcal{E}$, where the rows of \mathcal{E} are independent $N(0, \epsilon^2 I_2)$ distributed. The parameter ϵ affects the signal-to-noise ratio.

To facilitate comparison with traditional seriation methods, which rely on pairwise comparisons, we construct a comparison matrix $C \in \mathbb{R}^{N \times N}$. Using geodesic distances is powerful but they are impractical to obtain. We instead use the Euclidean distances from a reference point. Setting the reference point to be the origin $(0, 0)$, the entries of C are defined as

$$C(i, j) = 1_{|Z_i| < |Z_j|} - 1_{|Z_i| > |Z_j|}. \quad (12)$$

The goal is to determine the permutation $\pi : [N] \rightarrow [N]$ such that $t_{\pi(i)}$ is monotone increasing. We compare our approach Algorithm 1 with a traditional seriation method in Fogel et al. (2014); see Algorithm 1 therein. For our method, we use a bandwidth $\sigma^2 = 0.05$ for (a) and $\sigma^2 = 0.005$ for (b). The comparison approach Fogel et al. (2014) is applied on the comparison matrix C . For an estimator $\hat{\pi}$, the relative error is defined as

$$Err(\hat{\pi}, \pi) = \|\hat{\pi} \circ X - \pi \circ X\|_F / \|X\|_F, \quad (13)$$

where π is the truth and $\pi \circ X$ denote the re-arranged matrix with the i -th row being $X(\pi(t_i))$. For this open curve case, $Err(\hat{\pi}, \pi)$ is calculated for the data points with temporal label $t_i \in (0.05 * b, 0.95 * b)$, where $b = \pi$ for (a) and $b = 8\pi/5$ for (b).

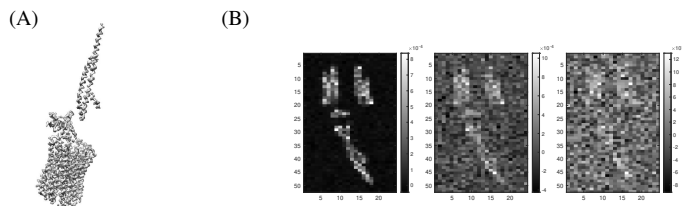


Figure 2: (A) One isosurface of the molecule. (B) The central slice of the molecule masked by Gaussian noise with SNR being 100, 1 and 0.2 in left, middle, and right panels, respectively.

Define the signal-to-noise ratio $SNR = \|X\|_F^2 / \|\mathcal{E}\|_F^2$. We evaluate the performance of two approaches across a range of SNR values from 0.1 to 1000, increasing in increments of 20. The relative error $Err(\hat{\pi}, \pi)$ is shown in Figure 1, with the results averaged over 20 repetitions. The performances of both methods are comparable in scenario (a), where Euclidean distances provide reasonable pairwise comparisons. However, in scenarios like (b), where Euclidean distances fail to accurately reflect geodesic ordering, our method significantly outperforms the approach described in Fogel et al. (2014), and achieves similar relative errors as the half-circle case.

4.2 Simulation studies on molecule data

We consider the sorting problem for voxel data of a biological molecule undergoing a rotation, which is essentially one-dimensional. The original voxel data used in Zelesko et al. (2019) represents the density map of an electric motor in adenosine triphosphate synthase, with a size of $24 \times 52 \times 24$ after downsampling. Upon vectorizing the voxel data, the dimensionality is established at $d = 29952$.

We generate data for the case the molecule is taking 3D rotations around the y -axis. We sample rotation angles, i.e. temporal labels t_i , uniformly from $[0, \pi]$ for the open curve scenario and $[0, 2\pi)$ for the closed loop scenario. For each scenario, we form a clean data matrix $X \in \mathbb{R}^{N \times d}$ whose rows are the vectorization of rotated voxel data at the sampled angle t_i . Then we get a noisy data matrix $Z = X + \mathcal{E}$ by adding i.i.d. Gaussian noise with variance ϵ^2 on each entry. An example of the isosurface of this biological molecule and the central slice of the molecule contaminated by different levels of noise is shown in Figure 2.

The first study aims to demonstrate that the second (and third) Fiedler vector(s) by Algorithm 1 (and 2) exhibit intrinsic geometry resembling 1D manifolds. In both cases, we first denoise Z by Algorithm 4. Typically, it reduces the high dimensional $d = 29952$ to a comparatively low dimension r , usually in the range $r \in [200, 300]$. For the denoised data, we then apply Algorithms 1 and 2 under the open curve case and closed loop case, respectively. In both scenarios, the bandwidth is $\sigma^2 = 0.005$. We consider different combinations of the sample size $N = 500, 5000, 50000$ and $SNR = 0.2, 1, 100$, where $SNR = \|X\|_F^2 / \|\mathcal{E}\|_F^2$.

The entries of the second Fiedler vector versus angles t_i for the open curve case are visualized in Figure 3(A), and the scatter plot of the entries of the second and third

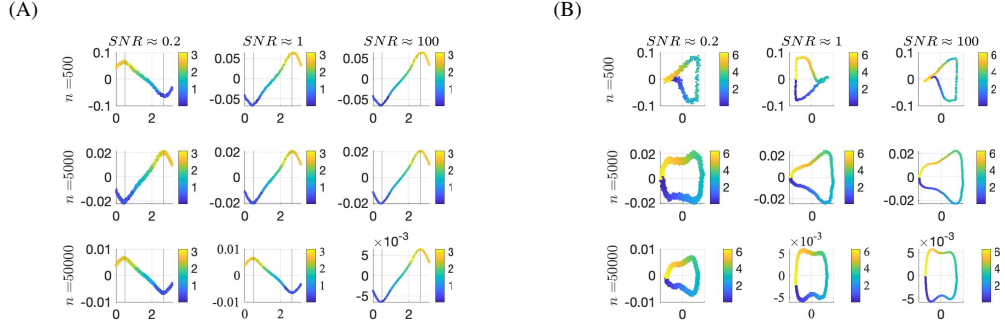


Figure 3: Left: The second Fiedler vector versus angles under the open curve case. Right: The second versus the third Fiedler vector under the closed loop case.

Fiedler vectors for the closed loop cases is presented in Figure 3(B). The results suggest that Fiedler vectors can estimate the angles well, up to a possible reflection and rotation (for closed loop case only). It illustrates the intuition of using Fiedler vectors to recover the angles. When SNR and N increase, the angles are easier to identify by the Fiedler vectors. However, as we point out, there are large errors around the two endpoints in the open curve case, even with large N and SNR.

The second study about this example is to evaluate the performance of our seriation approach. For $N \in \{100, 1000, 10000\}$ and $\text{SNR} \in [10^{-2}, 10^5]$, we denoise the data and apply our approach to obtain the estimated rankings $\hat{\pi}$. To optimize performance, we employ a data-dependent approach to select the bandwidth σ for each data matrix, as described in Section 6.2.1 of Harlim (2018). The average relative error $Err_X(\pi, \hat{\pi})$ is calculated by (13) over 20 replicates. We then fix $\text{SNR} \in \{0.2, 1, 100\}$ and let $N \in [100, 10000]$. Results are presented in Figure 4.

For both scenarios, our seriation method can achieve a small relative error when N is sufficiently large and SNR is at a moderate scale. However, for small N , increasing SNR cannot perfectly solve the problem because of the “essential error” at $\tilde{O}(N^{-1/14})$ for the open curve case and $\tilde{O}(N^{-2/7})$ for the closed loop case. The same thing happens when SNR is fixed and N increases. It is consistent with our theoretical results, presenting separate terms on N and ϵ .

Acknowledgement

Yuehaw Khoo’s research is partially supported by DMS-2111563, DMS-2339439, DE-SC0022232. Xin T. Tong’s research is supported by Singapore MOE grant Tier-1-A-8000459-00-00. Wanjie Wang’s research is supported by Singapore MOE grant Tier-1-A-8001451-00-00. Yuguan Wang’s research is supported by the Department of Statistics, University of Chicago. The authors thank John Harlim and Xiuyuan Cheng for their valuable comments and discussions.

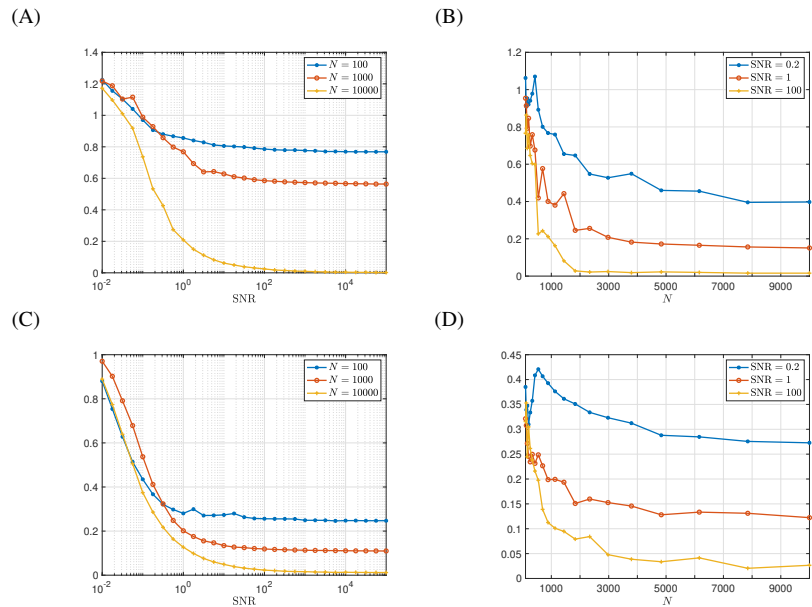


Figure 4: Relative errors $Err_X(\pi, \hat{\pi})$ under the closed loop case (first row) and the open curve case (second row).

Supplementary material

Supplementary material available at *Biometrika* online includes theoretical proofs of theorems.

A Appendix: PCA matrix denoising for high-dimensional data

In challenging settings, Assumption 3 that $\|Z_i - X(t_i)\| \leq \epsilon$ may not hold. For example, for diverging d , a high-dimensional noise $e_i \sim N(0, \epsilon^2 I_d)$ has a uniform bound $\|e_i\| \approx \sqrt{d \log N} \epsilon$ and hence ruin the convergence of eigenvectors. In this section, we introduce a denoising algorithm for Z . A full discussion on the uniform error control of this denoising algorithm can be found in Tong et al. (2023).

A popular denoising method is to project the data into the eigen-space. Suppose X has a low rank of $\text{rank}(X) = r \ll d$. Let $U \in \mathbb{R}^{d \times r}$ be the matrix formed by the first r left singular vectors of X and $\text{col}(U)$ be the eigen-space spanned by columns of U . The projection of X into $\text{col}(U)$ remains X , i.e. $UU^T X = X$, while $UU^T \mathcal{E}$ largely reduces the magnitude of noise. Without the access of X and hence U , we use the singular value decomposition of Z to get \tilde{U} and denoising data $\tilde{Z} = \tilde{U}\tilde{U}^T Z$, as below.

Algorithm 3 *Denoise and compress noisy high-dimensional data*

Input: noisy data $Z \in \mathbb{R}^{d \times N}$, rank $r \ll d$.

1. Let $\tilde{U} = (u_1, \dots, u_r) \in \mathbb{R}^{d \times r}$ be the matrix formed by left singular vectors of Z , corresponding to the largest r singular values.
2. Denoise the data points by $\tilde{Z}_i = \tilde{U}\tilde{U}^T Z_i$ and hence $\tilde{Z} = \tilde{U}\tilde{U}^T Z \in \mathbb{R}^{d \times N}$.

Output: denoised data points $\tilde{Z}_i \in \mathbb{R}^d$, $i \in [N]$.

When $\text{rank}(X) = r \ll d$, the denoised data has a uniform error bound that $\max_i \|\tilde{Z}_i - X(t_i)\| = \tilde{O}(\epsilon\sqrt{r})$ when $e_i \sim \mathcal{N}(0, \epsilon^2 I_d)$ by Tong et al. (2023). It is a significant improvement compared to the uniform error bound for the original data $\max_i \|Z_i - X(t_i)\| = \tilde{O}(\epsilon\sqrt{d})$.

In real data, the rank of X is unknown, but an upper bound $r_0 \geq r$ is usually available. We use a variant of the randomized range finding algorithm in Halko et al. (2011) to estimate r and find \tilde{U} , based on Z and an over-sampling rank parameter r_0 . The idea is to take the product of Z and a noise matrix $G \in \mathbb{R}^{N \times r_0}$, so that the eigenspace formed by left singular vectors remains the same, while the singular values are affected by the additional randomization G . The estimation of r corresponds to the rank of the first singular value of ZG that is significantly smaller compared to the largest singular value of ZG . Details in Algorithm 4.

Algorithm 4 *Denoise and compress noisy high-dim data with over-sampling rank r_0 .*

Input: noisy data $Z \in \mathbb{R}^{d \times N}$, over-sampling rank $r_0 \ll d$, tuning parameter η .

1. Generate a Gaussian random matrix $G \in \mathbb{R}^{N \times r_0}$ and let $Y = ZG \in \mathbb{R}^{d \times r_0}$.
2. Compute the singular value decomposition of $Y = U\Sigma V^T$.
3. Let $\lambda_k(Y)$ be the k -th largest singular values.
Estimate the rank $\hat{r} = \min \{1 \leq i \leq r_0 \mid \lambda_i(Y)/\lambda_1(Y) < \eta\}$.
4. Let \tilde{U} be $d \times \hat{r}$ matrix formed by the first \hat{r} singular vectors in U .
5. Denoise the data points by $\tilde{Z}_i = \tilde{U}\tilde{U}^T Z_i$ and hence $\tilde{Z} = \tilde{U}\tilde{U}^T Z \in \mathbb{R}^{d \times N}$.

Output: estimated rank \hat{r} and denoised data matrix $\tilde{Z} \in \mathbb{R}^{d \times N}$.

Remark 5 *The tuning parameter η is a very small constant to guarantee the leftover singular vectors are mainly noise. In numerical analysis of the molecule data, we take the over-sampling rank $r_0 = 400$ and $\eta = 10^{-3}$. The estimated rank r is between 200 and 300 in repetitions.*

Combining Algorithm 4 and Algorithms 1–2 gives us the outline of the temporal label recovery algorithm for high-dimensional data: first get the denoised data matrix \tilde{Z} , then apply the spectral method on \tilde{Z} in place of Z . We apply this approach in Section 4.2 and get satisfactory results.

References

- ABBE, E., FAN, J., WANG, K. & ZHONG, Y. (2020). Entrywise eigenvector analysis of random matrices with low expected rank. *Annals of statistics* **48**, 1452.
- ABBE, E. & SANDON, C. (2015). Community detection in general stochastic block models: Fundamental limits and efficient algorithms for recovery. In *2015 IEEE 56th Annual Symposium on Foundations of Computer Science*. IEEE.
- ARABIE, P., HUBERT, L. & DE SOETE, G. (1996). An overview of combinatorial data analysis. *Clustering and classification* , 5.
- ASCH, M., BOCQUET, M. & NODET, M. (2016). *Data assimilation: methods, algorithms, and applications*. SIAM.
- ATKINS, J. E., BOMAN, E. G. & HENDRICKSON, B. (1998). A spectral algorithm for seriation and the consecutive ones problem. *SIAM Journal on Computing* **28**, 297–310.
- BAILER-JONES, C. A., MACKAY, D. J. & WITHERS, P. J. (1998). A recurrent neural network for modelling dynamical systems. *network: computation in neural systems* **9**, 531.
- BROWN, C. T., OLM, M. R., THOMAS, B. C. & BANFIELD, J. F. (2016). Measurement of bacterial replication rates in microbial communities. *Nature biotechnology* **34**, 1256–1263.
- BRUSCO, M. J., STAHL, S. et al. (2005). *Branch-and-bound applications in combinatorial data analysis*, vol. 2. Springer.
- CAI, T. T. & MA, R. (2023). Matrix reordering for noisy disordered matrices: Optimality and computationally efficient algorithms. *IEEE Transactions on Information Theory* .
- CAI, T. T. & ZHANG, A. (2018). Rate-optimal perturbation bounds for singular subspaces with applications to high-dimensional statistics. *Annals of Statistics* **46**, 60–89.
- CHEN, Y., CHI, Y., FAN, J., MA, C. et al. (2021). Spectral methods for data science: A statistical perspective. *Foundations and Trends® in Machine Learning* **14**, 566–806.
- CHENG, X. & WU, N. (2022). Eigen-convergence of gaussian kernelized graph laplacian by manifold heat interpolation. *Applied and Computational Harmonic Analysis* **61**, 132–190.
- COIFMAN, R. R. & LAFON, S. (2006). Diffusion maps. *Applied and computational harmonic analysis* **21**, 5–30.
- COSSIO, P. et al. (2022). Extracting free-energy profiles from cryo-electron microscopy experiments. *Acta Crystallographica Section A: Foundations and Advances* **78**, a117–a117.

- DAVIS, C. & KAHAN, W. M. (1970). The rotation of eigenvectors by a perturbation. iii. *SIAM Journal on Numerical Analysis* **7**, 1–46.
- DSILVA, C. J., LIM, B., LU, H., SINGER, A., KEVREKIDIS, I. G. & SHVARTSMAN, S. Y. (2015). Temporal ordering and registration of images in studies of developmental dynamics. *Development* **142**, 1717–1724.
- DUNSON, D. B., WU, H.-T. & WU, N. (2021). Spectral convergence of graph laplacian and heat kernel reconstruction in l^∞ from random samples. *Applied and Computational Harmonic Analysis* **55**, 282–336.
- FOGEL, F., D’ASPROMONT, A. & VOJNOVIC, M. (2014). Serialrank: Spectral ranking using seriation. *Advances in Neural Information Processing Systems* **27**.
- GARCÍA TRILLOS, N., GERLACH, M., HEIN, M. & SLEPCEV, D. (2020). Error estimates for spectral convergence of the graph laplacian on random geometric graphs toward the laplace–beltrami operator. *Foundations of Computational Mathematics* **20**, 827–887.
- HAHSLER, M., HORNIK, K. & BUCHTA, C. (2008). Getting things in order: an introduction to the r package seriation. *Journal of Statistical Software* **25**, 1–34.
- HALKO, N., MARTINSSON, P. G. & TROPP, J. A. (2011). Finding structure with randomness: Probabilistic algorithms for constructing approximate matrix decompositions. *SIAM Review* **53**, 217–288.
- HAMILTON, J. D. (2020). *Time series analysis*. Princeton university press.
- HARLIM, J. (2018). *Data-Driven Computational Methods: Parameter and Operator Estimations*. Cambridge University Press.
- HU, Y. & WANG, W. (2024). Network-adjusted covariates for community detection. *Biometrika*, asae011.
- HUBERT, L., ARABIE, P. & MEULMAN, J. (2001). *Combinatorial data analysis: Optimization by dynamic programming*. SIAM.
- JAEGER, J., SURKOVA, S., BLAGOV, M., JANSSENS, H., KOSMAN, D., KOZLOV, K. N., MYASNIKOVA, E., VANARIO-ALONSO, C. E., SAMSONOVA, M., SHARP, D. H. et al. (2004). Dynamic control of positional information in the early drosophila embryo. *Nature* **430**, 368–371.
- LAW, K., STUART, A. & ZYGALAKIS, K. (2015). Data assimilation. *Cham, Switzerland: Springer* **214**, 52.
- LEDERMAN, R. R., ANDÉN, J. & SINGER, A. (2020). Hyper-molecules: on the representation and recovery of dynamical structures for applications in flexible macromolecules in cryo-em. *Inverse problems* **36**, 044005.
- MA, R., CAI, T. T. & LI, H. (2021a). Optimal estimation of bacterial growth rates based on a permuted monotone matrix. *Biometrika* **108**, 693–708.

- MA, R., CAI, T. T. & LI, H. (2021b). Optimal permutation recovery in permuted monotone matrix model. *Journal of the American Statistical Association* **116**, 1358–1372.
- MOSCOVICH, A., HALEVI, A., ANDÉN, J. & SINGER, A. (2020). Cryo-em reconstruction of continuous heterogeneity by laplacian spectral volumes. *Inverse Problems* **36**, 024003.
- O'BRIEN, M. J. & LYMAN, R. L. (1999). *Seriation, stratigraphy, and index fossils: The backbone of archaeological dating*. Springer Science & Business Media.
- PEOPLES, J. W. & HARLIM, J. (2021). Spectral convergence of symmetrized graph laplacian on manifolds with boundary. *arXiv preprint arXiv:2110.06988*.
- RIGOLLET, P. & WEED, J. (2019). Uncoupled isotonic regression via minimum wasserstein deconvolution. *Information and Inference: A Journal of the IMA* **8**, 691–717.
- ROSENBERG, S. (1997). *The Laplacian on a Riemannian manifold: an introduction to analysis on manifolds*. No. 31 in London Mathematical Society Student Texts. Cambridge University Press.
- SEITZ, E., ACOSTA-REYES, F., MAJI, S., SCHWANDER, P. & FRANK, J. (2022). Recovery of conformational continuum from single-particle cryo-em images: Optimization of manifoldem informed by ground truth. *IEEE transactions on computational imaging* **8**, 462–478.
- SELVIN, S., VINAYAKUMAR, R., GOPALAKRISHNAN, E., MENON, V. K. & SOMAN, K. (2017). Stock price prediction using lstm, rnn and cnn-sliding window model. In *2017 international conference on advances in computing, communications and informatics (icacci)*. IEEE.
- SHENNAN, S. (1997). *Quantifying archaeology*. University of Iowa Press.
- SINGER, A. (2006). From graph to manifold laplacian: The convergence rate. *Applied and Computational Harmonic Analysis* **21**, 128–134.
- SINGER, A. & SHKOLNISKY, Y. (2011). Three-dimensional structure determination from common lines in cryo-em by eigenvectors and semidefinite programming. *SIAM journal on imaging sciences* **4**, 543–572.
- TONG, X. T., WANG, W. & WANG, Y. (2023). Pca matrix denoising is uniform. *arXiv preprint arXiv:2306.12690*.
- TSAY, R. S. (2005). *Analysis of financial time series*. John wiley & sons.
- VANT, J. W., SARKAR, D., NGUYEN, J., BAKER, A. T., VERMAAS, J. V. & SINGHARROY, A. (2022). Exploring cryo-electron microscopy with molecular dynamics. *Biochemical Society Transactions* **50**, 569–581.

- WANG, W., TRIPATHY, S. J., PADMANABHAN, K., URBAN, N. N. & KASS, R. E. (2015). An empirical model for reliable spiking activity. *Neural computation* **27**, 1609–1623.
- YOSHIDA, M., MUNAYUKI, E. & HISABORI, T. (2001). Atp synthase—a marvellous rotary engine of the cell. *Nature Reviews Molecular Cell Biology* **2**, 669–677.
- ZELESKO, N., MOSCOVICH, A., KILEEL, J. & SINGER, A. (2019). Earthmover-based manifold learning for analyzing molecular conformation spaces. *2020 IEEE 17th International Symposium on Biomedical Imaging (ISBI)*, 1715–1719.